NeuroImage: Clinical 17 (2018) 31–42

Contents lists available at ScienceDirect

NeuroImage: Clinical

journal homepage: www.elsevier.com/locate/ynicl

Aberrant brain functional connectivity in newborns with congenital heart disease before cardiac surgery

Josepheen De Asis-Cruz[a], Mary T. Donofrio[b], Gilbert Vezina[a], Catherine Limperopoulos[a,*]

[a] Division of Diagnostic Imaging and Radiology, Children's National Health System, Washington, D.C. 20010, USA
[b] Division of Cardiology, Children's National Health System, Washington, D.C. 20010, USA

ARTICLE INFO

Keywords:
Congenital heart disease
Neurodevelopment
Neonatal resting state networks
Graph theory

ABSTRACT

Newborns with congenital heart disease (CHD) requiring open heart surgery are at increased risk for neurodevelopmental disabilities. Recent quantitative MRI studies have reported disrupted growth, microstructure, and metabolism in fetuses and newborns with complex CHD. To date, no study has examined whether functional brain connectivity is altered in this high-risk population after birth, before surgery. Our objective was to compare whole-brain functional connectivity of resting state networks in healthy, term newborns (n = 82) and in term neonates with CHD before surgery (n = 30) using graph theory and network-based statistics. We report for the first time intact global network topology – efficient and economic small world networks – but reduced regional functional connectivity involving critical brain regions (i.e. network hubs and/or rich club nodes) in newborns with CHD before surgery. These findings suggest the presence of early-life brain dysfunction in CHD which may be associated with neurodevelopmental impairments in the years following cardiac surgery. Additional studies are needed to evaluate the prognostic, diagnostic and surveillance potential of these findings.

1. Introduction

Congenital heart disease (CHD) affects brain development across the lifespan. While long-term survival after neonatal cardiac surgery has dramatically improved, the risk for neurodevelopmental impairments remain largely unchanged (Gaynor et al., 2015). Neurodevelopmental disabilities affect over 50% (McQuillen et al., 2007) of surviving infants with CHD and involve multiple domains, including motor function, learning, social behavior, and executive function (Donofrio and Massaro, 2010; Marelli et al., 2016). Early studies proposed intraoperative procedures, such as prolonged cardiopulmonary arrest time (Bellinger et al., 1995; Hövels-Gürich et al., 2002) and the cardiac bypass procedure itself (Newman et al., 2001), as major risk factors for brain injury in CHD. While these factors may contribute to future neurologic impairment, neurobehavioral evaluation in newborns with CHD before open heart surgery have demonstrated neurologic dysfunction in more than half of infants (Limperopoulos et al., 1999, 2002). Notably, these pre-operative findings have been found to be important independent baseline predictors for later neurodevelopmental dysfunction. Recently, advanced neuroimaging studies have provided further evidence for delayed brain growth and structural brain injury in CHD infants before surgery (Clouchoux et al., 2013; Limperopoulos et al., 2010; Miller et al., 2007) providing accruing evidence for the origin and evolution of brain dysfunction in this high-risk group.

Magnetic resonance imaging (MRI) has played a pivotal role in advancing our understanding of the onset, progression and mechanisms of brain injury in CHD. Conventional MRI studies have reported clinically-silent white matter lesions in newborns CHD before surgery, akin to those observed in premature brains (Miller et al., 2004). More importantly, advanced, quantitative MRI approaches such as magnetic resonance spectroscopy (MRS) and diffusion tensor imaging (DTI) have revealed alterations in biochemistry and microstructure in CHD when there are none evident on conventional MRI. Specifically, MRS has revealed decreased *N*-acetylaspartate (NAA) and the presence of lactate, suggesting neuronal loss and increased anaerobic metabolism, respectively (Miller et al., 2007). In contrast to focal white matter injury detected on conventional MRI, DTI has revealed diffuse white matter injury (reduced fractional anisotropy, FA), a finding consistent with the wide spectrum of neurodevelopmental abnormalities seen in surviving infants with CHD. More recently, in utero quantitative MRI studies in CHD fetuses provides further support for third trimester disturbances in brain growth, alterations in cortical gyrification and sulcation, as well as impaired cerebral metabolism (Clouchoux et al., 2013; Limperopoulos et al., 2010).

However, the extent to which alterations in brain structure and

* Corresponding author at: Children's National Health System, 111 Michigan Ave. N.W., Washington, D.C. 20010, USA.
E-mail address: climpero@childrensnational.org (C. Limperopoulos).

http://dx.doi.org/10.1016/j.nicl.2017.09.020
Received 16 June 2017; Received in revised form 13 September 2017; Accepted 25 September 2017
Available online 28 September 2017

metabolism in CHD are accompanied by brain circuitry dysfunction has yet to be explored. In this study, we used resting state functional connectivity MRI (rs-fcMRI) to compare brain connectivity in neonates with CHD before open heart surgery to full-term healthy control newborns. Resting state functional connectivity MRI provides critical insights into brain function by detecting temporal correlations between intrinsic, low frequency fluctuations of blood oxygen level dependent (BOLD) signals from different areas of the brain (Biswal et al., 1995). Neuropsychiatric disorders (i.e. autism spectrum disorder, attention deficit hyperactivity disorder, and schizophrenia), have been linked with disrupted large-scale network organization defined by rs-fcMRI and clinical measures of disease severity (Itahashi et al., 2014; Lynall et al., 2010) or presence/absence of disease (Moseley et al., 2015). In addition, we and others have described the organization of resting state networks in healthy, term newborns (De Asis-Cruz et al., 2015; Fransson et al., 2011; Gao et al., 2011). In this study, we used rs-fcMRI to characterize functional network organization in the developing CHD brain. To the best of our knowledge, this is the first rs-fcMRI study to examine the effects of CHD on brain function after birth, before open heart surgery. We hypothesized that newborns with CHD with no evidence of structural brain injury on conventional MRI would demonstrate connectivity disturbances involving multiple brain regions, akin to the diffuse white matter changes observed with DTI. To test this hypothesis, we used two complementary approaches. First, we characterized global, intermediate and local network organization in CHD compared to control networks using graph theoretic techniques. Second, we used network-based statistics (NBS) to delineate whole-brain simple functional connectivity, evaluating temporal correlations between BOLD signals from regions of interest (ROIs).

2. Materials and methods

2.1. Subjects

We acquired T2-weighted and resting state EPI data from 138 term neonates – 43 with CHD before open-heart surgery and 95 healthy controls – as part of an ongoing prospective observational study examining brain growth and development in fetuses and newborns with complex CHD. See Supplementary Table 1 for exclusion criteria. Resting state data from 23 newborns, 10 CHD and 13 controls, were excluded from further analysis for failing initial quality checks (see Preprocessing of functional images). Conventional MRI scans of the remaining 115 infants, were reviewed by an expert pediatric neuroradiologist (G.V.) who was blinded to group (CHD vs control) and clinical course of CHD infant. Data from three subjects were excluded. Two CHD newborns had parenchymal brain injury before cardiac surgery, specifically cerebellar punctate hemorrhage (1) and a small infarct in the left striatum and posterior limb of the internal capsule (1); one had cerebellar hypoplasia. The remaining 30 CHD and 82 control newborns had structurally normal brain MRI scans and underwent rs-fcMRI analyses. Neonates with CHD were delivered and scanned earlier compared to controls, had lower birth weights and lower APGAR scores at 1 and 5 min ($p < 0.05$ for all). The APGAR score is a means for rapidly assessing a newborn's health; it stands for **A**ppearance (skin color), **P**ulse (heart rate), **G**rimace (reflex irritability), **A**ctivity (muscle tone), and **R**espiration. Table 1 details characteristics of cohorts.

Parental informed consent was obtained for all newborns prior to the study. This study was approved by the Institutional Review Board (IRB) of the Children's National Health System. All experiments were performed in accordance with the regulations and guidelines of the Children's National Health System IRB.

2.2. Data acquisition

All MRI data were acquired using a 3 T GE scanner (Discovery MR750, GE Healthcare, Milwaukee, WI) using an 8-channel infant head coil. Prior to scanning, infants were fed, swaddled in a warm blanket, immobilized using an infant vacuum pillow, and provided ear protection using silicone ear plugs and adhesive ear muffs. Their physiologic state (i.e. heart rate and oxygen saturation) was monitored by a nurse throughout the scan. All control newborns were scanned unsedated while three CHD neonates were sedated during their preoperative scan. All infants (controls and CHD) underwent the exact same MRI protocol. Specifically, anatomical T2-weighted fast spin echo images were collected with the following parameters: TR = 2000 ms, TE = 64.49 ms, and voxel size = 0.625 × 1 × 0.625 mm. Resting state data were obtained using a T2-weighted gradient-echo planar imaging (EPI) sequence with parameters TR = 2000 ms, TE = 35 ms, voxel size = 3.125 × 3.125 × 3 mm, flip angle = 60°, field of view = 100 mm, and matrix size = 64 × 64. A total of 200 volumes - 6 min and 40 s of data - were collected. To achieve whole brain coverage, around 34 slices (range = 31–36), without slice gap, were obtained per subject.

Table 1
Demographic and clinical characteristics of cohorts.

	Control n = 82	CHD n = 30	*p* value[a]
Male sex (n)	44	17	0.8
GA at birth (wk)			0.002
Median	39.6	39	
Interquartile range	38.9–40.3	38.3–39.4	
PMA at preoperative MRI (wk)			8.9×10^{-12}
Median	41.5	39.4	
Interquartile range	40.7–42.1	38.9–39.7	
Birth weight (g)[b]			0.0502
Median	3337	3119	
Interquartile range	3070–3620	2940–3463	
APGAR score at 1 min[c]			0.003
Median	8	8	
Interquartile range	8–9	8–8	
APGAR score at 5 min (n)[c]			2.2×10^{-6}
Median	9	9	
Interquartile range	9–9	8–9	
Cardiac lesion			
Single-ventricle defects (n)			
Hypoplastic left heart syndrome	–	10	–
Two-ventricle physiology (n)			
Transposition of the great vessels	–	7	–
Double outlet right ventricle	–	4	–
Atrioventricular septal defect	–	3	–
Coarctation of the aorta	–	2	–
Tetralogy of Fallot	–	1	–
Ventricular septal defect	–	1	–
Pulmonary atresia	–	1	–
Ebstein's anomaly	–	1	–
Preoperative mechanical ventilation	–	15	–
Lowest pH prior to MRI[d]			
Median	–	7.32	–
Interquartile range	–	7.29–7.35	–
Lowest pO_2 prior to MRI (mm Hg)[d]			
Median	–	34.1	–
Interquartile range	–	28.1–42.4	–
Highest pCO_2 prior to MRI (mm Hg)[d]			
Median	–	38.9	–
Interquartile range	–	35–46	–
Lowest O_2 saturation prior to MRI (%)[d]			
Median	–	62.5	–
Interquartile range	–	51.3–70	–

[a] All Between-group comparisons, except for gender done using Mann-Whitney *U* Test; sex comparison performed using (Fisher's exact test).
[b] Birthweight not available for 1 control newborn; missing data replaced with median birth weight for the control cohort.
[c] Apgar scores not available for 5 controls; Apgar at 5 min not available for 1 CHD neonate.
[d] Pre-operative lowest pH, pO_2, pCO_2 and O_2 saturation levels not available for 5 CHD neonates; pO and O_2 saturation levels not available for two subjects.

2.3. Preprocessing of functional images

Functional MRI images were carefully inspected prior to preprocessing. Data from 21 neonates were excluded because of incomplete anatomical coverage (i.e., cerebellar cut-off), marked signal loss and obvious spatial distortions, and significant motion-related artifacts (i.e., ghosting).

Preprocessing was performed using AFNI software (Cox, 1996) unless otherwise noted. The first four echo-planar images were excluded to allow for signal equilibrium leaving 196 volumes for each subject. After removing large spikes from the data, in-plane motion (using slicewise motion correction/SLOMOCO) (Beall and Lowe, 2014)), slice-dependent temporal offsets and image inhomogeneities (Advanced Normalization ToolS N4 tool) (Tustison et al., 2010) were corrected. Functional volumes were then rigidly registered to a base EPI volume, intensity-scaled to a global mode of 1000 (Ojemann et al., 1997), and smoothed using a 6-mm full-width at half-maximum Gaussian blur. To attenuate the effects of non-neuronal signals on spontaneous BOLD fluctuations, averaged BOLD signals from white matter (WM) and cerebrospinal fluid (CSF), along with motion parameters and their derivatives were regressed out of the voxel-wise time series prior to smoothing. WM and CSF were defined in subjects' anatomical T2-weighted image using the DrawEM Segmentation Software Package (Makropoulos et al., 2014), part of the Medical Image Registration Toolkit or MIRTK, and registered to the subject's base EPI volume. The quality of co-registration of EPI and anatomical images was carefully examined visually. WM and CSF masks were eroded before signals were obtained to reduce the chances of removing BOLD signal from gray matter. Resting state data and noise signals were simultaneously bandpass filtered ($0.009 < f < 0.08$) before regression (Hallquist et al., 2013; Jo et al., 2013); residuals were used in subsequent functional connectivity and graph analyses.

To minimize motion-related effects on functional connectivity, volumes with a frame-wise displacement (FD) > 0.5 mm (Power et al., 2012) and with a high fraction of BOLD signal outliers (> 10% of voxels per volume; (Jo et al., 2013) were censored. Two CHD neonates had < 4 min of data or 120 volumes after censoring and were excluded. About 5.6 and 6.0 min of data were retained for CHD and control groups, respectively. The number of retained volumes ($p = 0.11$) was not significantly different between groups but head motion (FD: $p = 0.018$; total displacement or TD: $p = 0.034$) was significantly higher in CHD neonates (Supplementary Table 2).

BOLD time courses over all voxels in 93 ROIs or nodes were measured (after intensity-based masking of label masks; (Peer et al., 2016)), averaged and analyzed. ROIs were applied to the EPI image using the same transformation used to align the T2 weighted image to the base EPI image. Intensity-based masking was used to ensure that voxels with significant signal dropout were excluded from the analysis. Ninety cortical and subcortical regions were defined using the Automated Anatomical Labelling (AAL) atlas mapped to neonates and infants (Shi et al., 2011) and combined with parcellation of the cerebellum (left and right) and brainstem from DrawEM. See Supplementary Table 3 for ROIs and their abbreviations.

2.4. Network topology

Complex network measures were computed using the publicly available Brain Connectivity Toolbox for MATLAB (Rubinov and Sporns, 2010).

2.4.1. Global network properties

Each subject's graph consisted of 93 nodes and their respective edges. These correspond to the 93 regions of interest (ROIs) and the Pearson correlations (r) between BOLD signals of all possible ROI pairs, respectively. To exclude spurious connections, only positive correlations significant at adjusted $p_{FDR} < 0.05$ were retained. To ensure reliable estimates of network topology, we included graphs where (2) at least 95% of the nodes were connected for at least 95% of subjects and (2) degree, $k > 2\ \ln(\text{number of nodes})$ (Achard et al., 2006; Bassett et al., 2006). Graphs defined in the correlation range $r = 0.19$–0.49 and connection density range $\kappa = 0.14$–0.32 meet the above criteria. Global network measures were computed from individuals' 93 × 93 binary, undirected graphs, expressed as the average of measured graph metrics within the above ranges (Lynall et al., 2010), and reported as a function of both r and κ.

Global metrics include average clustering coefficient (Cl), characteristic path length (L), small world index (σ), global efficiency (E_{global}), local efficiency (E_{local}), and cost efficiency (CE). Cl refers to the tendency of neighbors of a node to cluster together; L is the average distance between any two pairs of nodes. Cl and L provide insights on functional segregation and integration, respectively. Small world topology reflects the balance between these two processes in complex networks – a balance that facilitates efficient processing of information among nodes in the network (Watts and Strogatz, 1998). Here, the tendency of networks to exhibit small world properties was quantified using the small world index, σ, the ratio of normalized values Cl_{norm} (γ) and L_{norm} (λ): $\sigma = \gamma/\lambda$, where $\gamma = Cl_{\text{neonate}}/Cl_{\text{random}}$ and $\lambda = L_{\text{neonate}}/L_{\text{random}}$(Humphries and Gurney, 2008). For each subject, 100 random networks that preserved the degree distribution of the original network were used. Networks were considered small world if $Cl_{\text{neonate}} \gg C_{random}$, $L_{neonate} \geq L_{random}$ and $\sigma > 1$. To further describe networks' small world behavior, we also computed network efficiency, economy and cost efficiency. E_{global} refers to how well information is transferred in a graph; it is inversely related to L; E_{local} measures how well a node's neighbors communicate among themselves after the node is removed. Small world networks have efficiencies intermediate to random and regular networks (Achard et al., 2006; Humphries et al., 2006). For this comparison, similar to random networks, 100 regular networks that preserve the degree distribution of the original graph were constructed. Regular networks, unlike random graphs, are highly ordered. CE reflects the relationship between E_{global} and network cost or κ: $CE = E_{global} - \kappa$.

Graph metrics derived from individual networks were adjusted for gestational age, day of life, gender, and motion (i.e. FD) prior to group comparisons. Adjusted residuals were compared using permutation testing: 100,000 iterations, two-tailed, $\alpha = 0.05$. Given the evolving nature of resting state networks during infancy (Fransson et al., 2011; Gao et al., 2011), age adjustment was performed to attenuate the possible effects of age differences between our groups, notwithstanding dealing with a narrow range of four weeks. Adjustment for gender and motion, specifically framewise displacement, was also performed as these variables have been reported to influence network topology (Gong et al., 2011; Satterthwaite et al., 2012) in older children and adults; the effects of gender and motion on network topology in early infancy have yet to be fully elucidated.

2.4.2. Intermediate network properties

To assess intermediate network topology, we described rich club organization, the tendency of highly connected nodes to connect with each other (van den Heuvel and Sporns, 2011). The extent to which networks exhibit rich club organization was measured using the rich club coefficient, ϕ (Colizza et al., 2006). This was computed from group matrices derived from averaged individual correlation matrices. Group matrices were evaluated at 14% density, the sparsest density at which networks were examined in individuals. A network exhibits rich club organization if (1) $\phi_{norm} > 1$ for a range of degrees (k), and (2) $\phi_{neonate} > \phi_{random}$ (assessed by permutation testing; (Bassett and Bullmore, 2009). Coefficients were normalized relative to ϕ derived from 10,000 comparable random networks per group. Rich club anatomy was evaluated at $k = 18$, the highest k value at which all subjects had data.

2.4.3. Local network properties

We used 3 centrality measures to describe the influence of individual nodes in the network: degree, closeness and betweenness (Freeman, 1978; Freeman et al., 1991; van den Heuvel and Sporns, 2013). Degree, *k*, refers to the number of nodes a region is connected to. Closeness refers to how easily a node can reach other nodes or its distance to other nodes. Betweenness refers to the number of shortest paths that traverse a node. Network hubs were defined as nodes that are ranked in the top 20% for two out of the three centrality measures. To assess the degree of influence of all nodes in the network, a total centrality score was computed by ranking the sum of ranks for degree, closeness and betweenness. A more central/influential node in the network will have high rank (i.e. closer to 1). Correlation between node rankings in the two cohorts was assessed using Kendall rank correlation coefficient. Centrality measures for the top, middle, and bottom third of nodes for each group were then compared using paired *t*-tests. Rich club and hub organization were visualized with the BrainNet Viewer (Xia et al., 2013).

2.5. Network-based statistics

Differences in simple functional connectivity (correlations) among the 93 ROIs between the two groups was estimated using the network-based statistics (NBS) toolbox for MATLAB (Zalesky et al., 2010). NBS detects a subnetwork of nodes where functional connectivity differs between groups using permutation testing (iterations = 10,000, $p < 0.05$, threshold $t = 3.00$) In NBS, selection of the test statistic threshold is arbitrary. To guide our choice, we experimented over a range of t values (2.5 to 3.5) and showed the results for $t = 3$. The effects shown at this threshold were present across a range of thresholds. Gestational age at birth, day of life at scan, gender, and FD were included as covariates.

3. Results

3.1. Small world architecture of functional connectivity networks

CHD newborn resting state networks showed small world topology. Fig. 1 shows group means for average clustering coefficient (*Cl*), characteristic path length (*L*), normalized *Cl* (γ) and *L* (λ), and small world index (σ) of control and CHD functional connectivity networks. Supplementary Tables 4 and 5 summarizes global network metrics and adjusted group means, respectively. Newborn network *Cl* and *L* were significantly greater than comparable random graphs: $Cl_{NEO} \gg Cl_{random}$ and $L_{NEO} > L_{random}$ ($p < 1 \times 10^{-6}$). In addition, $\sigma > 1$ for both CHD and control networks. There were no statistically significant between-group differences in σ, γ, and λ suggesting preserved global organization of functional brain networks in complex CHD. Similar findings were obtained using density-thresholded networks (Supplementary Tables 6 and 7).

Small world networks of CHD neonates, like healthy infants, were simultaneously efficient and economic. There were no significant differences in local (E_{loc}; $p = 0.21$) and global (E_{glob}; $p = 0.17$) efficiency between the two cohorts (Fig. 1C). As expected in networks with small world topology, the efficiency of newborn functional connectivity networks lay intermediate between regular and random graphs: $E_{glob\text{-}random} > E_{glob\text{-}NEO} > E_{glob\text{-}reg}$ and $E_{loc\text{-}random} < E_{loc\text{-}NEO} < E_{loc\text{-}reg}$. CHD and control networks' E_{glob} and E_{loc} were greater than network costs; cost efficiency (*CE*) was always positive. Both suggest network economy: an optimized trade-off between efficient information processing and wiring costs (Achard and Bullmore, 2007). In CHD, *CE* was maximal when cost is 0.21, when 898 out of 4278 of all possible

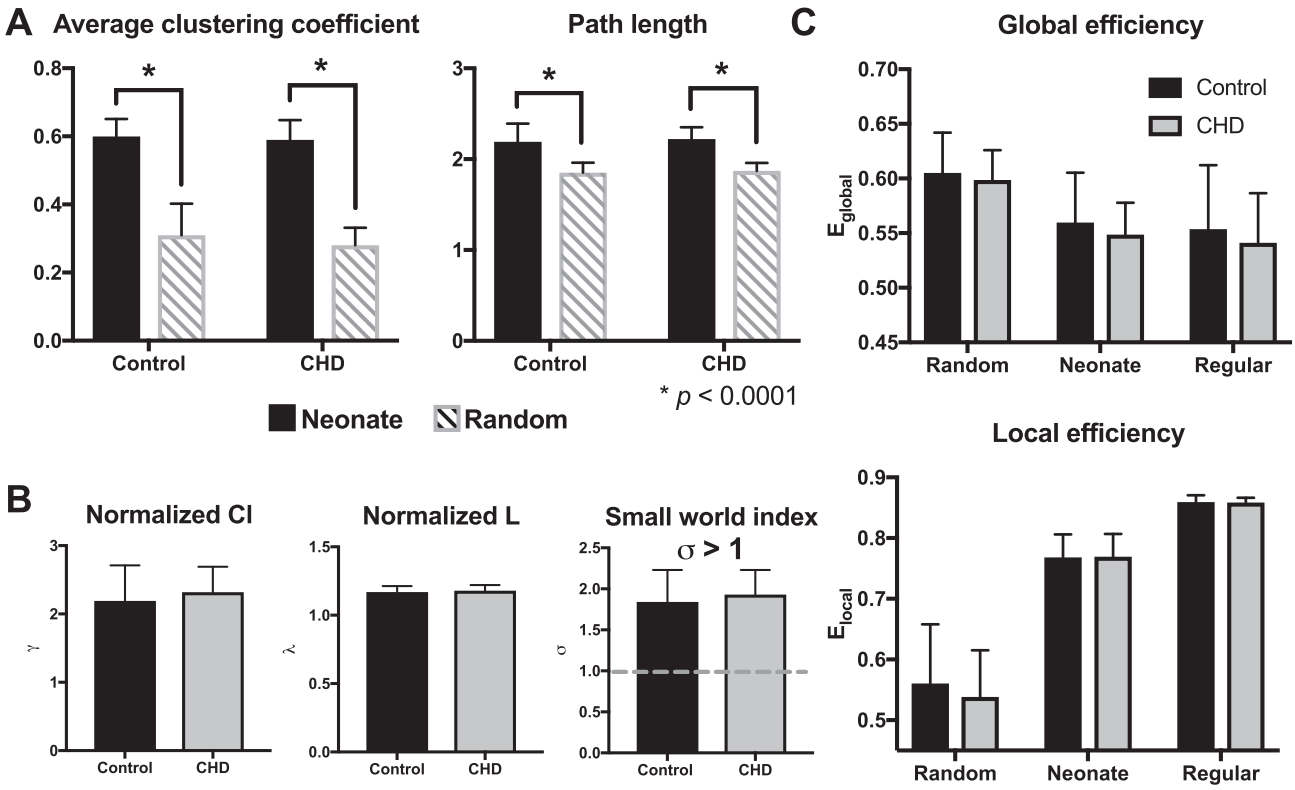

Fig. 1. Efficient, economic small world architecture preserved in neonates with CHD. (A) Bar plot of average clustering coefficient (Cl) and characteristic path length (L) of control and CHD resting state networks (black bars) relative to random networks (gray). In both groups, $Cl_{neonate} \gg Cl_{random}$ and $L_{neo} > L_{random}$. (B) Normalized clustering coefficient (γ), characteristic path length (λ) and small world indices (σ) are comparable between groups. Gray, dashed line marks the threshold for small world. (C) Efficiency of global and local networks fall between random and regular graphs, typical of small word networks in both CHD (gray) and controls (black). Global (E_{global}) and local (E_{local}) efficiency in CHD are comparable to controls. All metrics are averaged across Pearson *r* correlation thresholds 0.19–0.49.

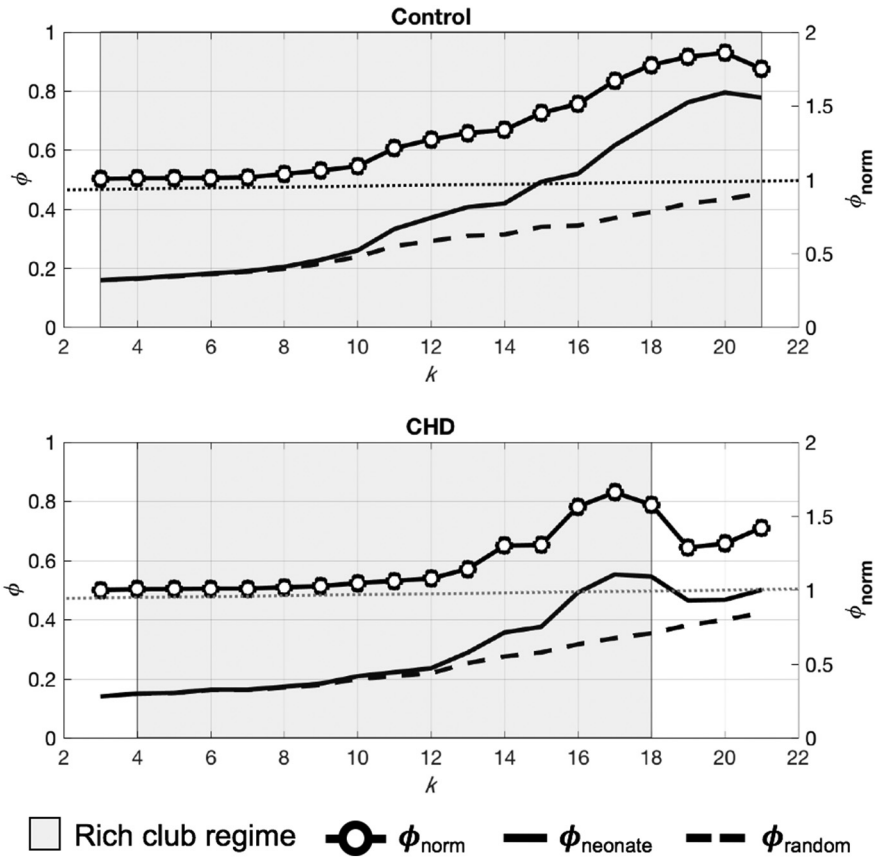

Fig. 2. Rich club organization in CHD and control newborns. Rich club organization preserved in CHD functional connectivity networks, but for a narrower (gray area) range of degree (k) values. $\phi_{norm} > 1$ suggest rich club organization (y axis on the right). ϕ_{norm}, normalized rich club coefficient; $\phi_{neonate}$, newborn networks' rich club coefficient; ϕ_{random}, random networks' rich club coefficient.

network connections were present. At this threshold, $CE_{CHD\text{-neo}}$ was 0.33. For controls, cost efficiency was highest, $CE_{ctrl\text{-}neo} = 0.33$, when edge density is 0.22 and 941 out of 4278 possible edges were present.

3.2. Rich club organization and anatomy

CHD functional connectivity networks showed rich-club organization like controls (Fig. 2). However, the range of degrees (k) at which the rich club regime was observed was narrower in CHD: k = 4–18 in CHD versus k = 3–21 in controls. This indicates denser connections among high degree nodes in the control group. For both cohorts within these k ranges, $\phi_{neonate} > \phi_{random}$ and $\phi_{norm} > 1$, fulfilling rich-club criteria. While both networks exhibit rich-club organization, where the cohorts' rich-club regimes overlapped, the rich club coefficients of controls were significantly greater than CHD ($p = 0.01$, paired t-test), suggesting reduced connections among rich-club nodes in CHD cohort.

Included in the rich-club anatomy are nodes with $k \geq 18$, the highest degree at which both groups exhibited rich club organization. The rich-club network of CHD neonates comprised 15 (16%) nodes, compared to 24 (26%) nodes observed in controls. Of the 15 rich-club regions in CHD, 14 were shared with controls, mostly limbic regions such as bilateral insulae, amygdalae, hippocampus and basal ganglia (i.e., bilateral putamen and left putamen). Fig. 3A shows the rich-club anatomy of both groups, highlighting areas of overlap and areas that are unique to each cohort. Supplementary Table 8 shows the list of rich club nodes with the matching degrees for each. The average degree of rich-club nodes in CHD (mean ± standard deviation, 20.3 ± 2.02) was not significantly lower ($p = 0.29$, 2-sample t-test) compared to controls (21.2 ± 3.00). However, there were more highly connected nodes (higher k) in controls compared to CHD (24 versus 15, as stated above).

3.3. Centrality of nodes in the CHD network

Hubs that were consistently ranked in the top 20% for all centrality measure in both CHD and controls included bilateral insulae, bilateral olfactory, and left posterior central gyrus. In total, there were 18 and 19 hubs for CHD and control networks, respectively (Fig. 3B), with 14 hubs common between the two groups.

Nodes with high centrality scores in controls were also ranked high in CHD ($r_\tau = 0.60$, $p = 2.30 \times 10^{-17}$; Fig. 4A). The ranking of nodes based on individual centrality measures were also highly correlated: degree, $r_\tau = 0.64$, $p = 4.6 \times 10^{-18}$; betweenness, $r_\tau = 0.47$, $p = 3.2 \times 10^{-18}$; and closeness, $r_\tau = 0.67$, $p = 8.8 \times 10^{-21}$. This suggests that highly influential nodes in controls – regions with numerous connections (high degree), close to other nodes (high closeness), and with a high number of short paths running through them (high betweenness) – will also be influential in CHD networks. Node rankings per group are listed in Supplementary Table 9. While the pattern in which hubs were ranked was similar in the two groups, nodes ranked in the top third in control networks had higher degree and closeness (Fig. 4B). The centrality hubs defined using the combined measures of degree, closeness, and betweenness were also consistent with the rich club nodes, which is defined by degree alone.

3.4. Subnetwork of brain regions with reduced connectivity in CHD

Using network-based statistics (NBS; (Zalesky et al., 2010), we identified a single subnetwork comprising 38 nodes sharing 60 edges with reduced connectivity in CHD ($p_{FDR} = 0.0005$; Fig. 5, left; Supplementary Tables 10 and 11 show affected edges and nodes, respectively, for other t values examined). This equates to 1.4% of all possible connections involving about 41% of the 93 nodes. Table 2 lists the degree or the number of connections of each affected ROI within the subnetwork and the affected edges sorted based on decreasing t-statistic

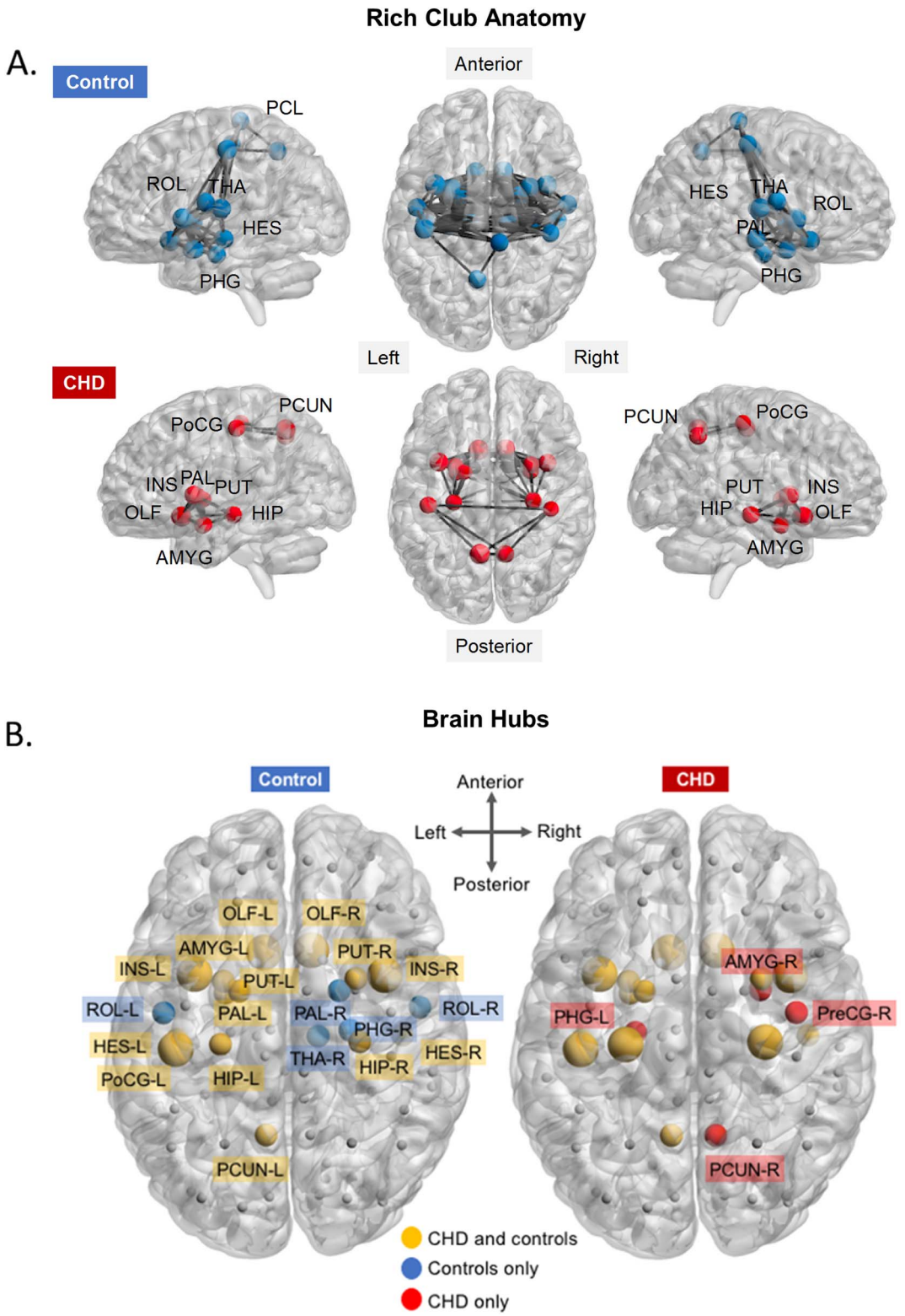

Fig. 3. CHD and control networks' rich club nodes and hubs. (A) Rich club anatomy in CHD and control networks. Note fewer rich club nodes in CHD (bottom panel; nodes, red spheres) compared to controls (top; nodes, blue spheres) and reduced connection density among rich club nodes in CHD (black lines). Rich club nodes common to the two groups are labeled in the bottom panel. Rich club nodes unique to a group are highlighted in yellow. (B) Network hubs based on degree, betweenness and closeness centrality. Yellow spheres are hubs common to both groups, blue are hubs in control networks and red are hubs in CHD networks. (For interpretation of the references to color in this figure legend, the reader is referred to the web version of this article.)

values. The functional correlations between affected ROIs were always lower in CHD compared to controls (Fig. 6, right). Subcortical areas and the brainstem were predominantly involved; the greatest differences in functional connectivity involved the globus pallidus, brainstem, and caudate. Of the 60 edges with reduced connectivity in CHD, 36 (60%) involved subcortical regions or brainstem and their connections with frontal, parietal and temporal cortices (23/36 or 64% of edges from subcortical regions). Overall, excluding connections involving the

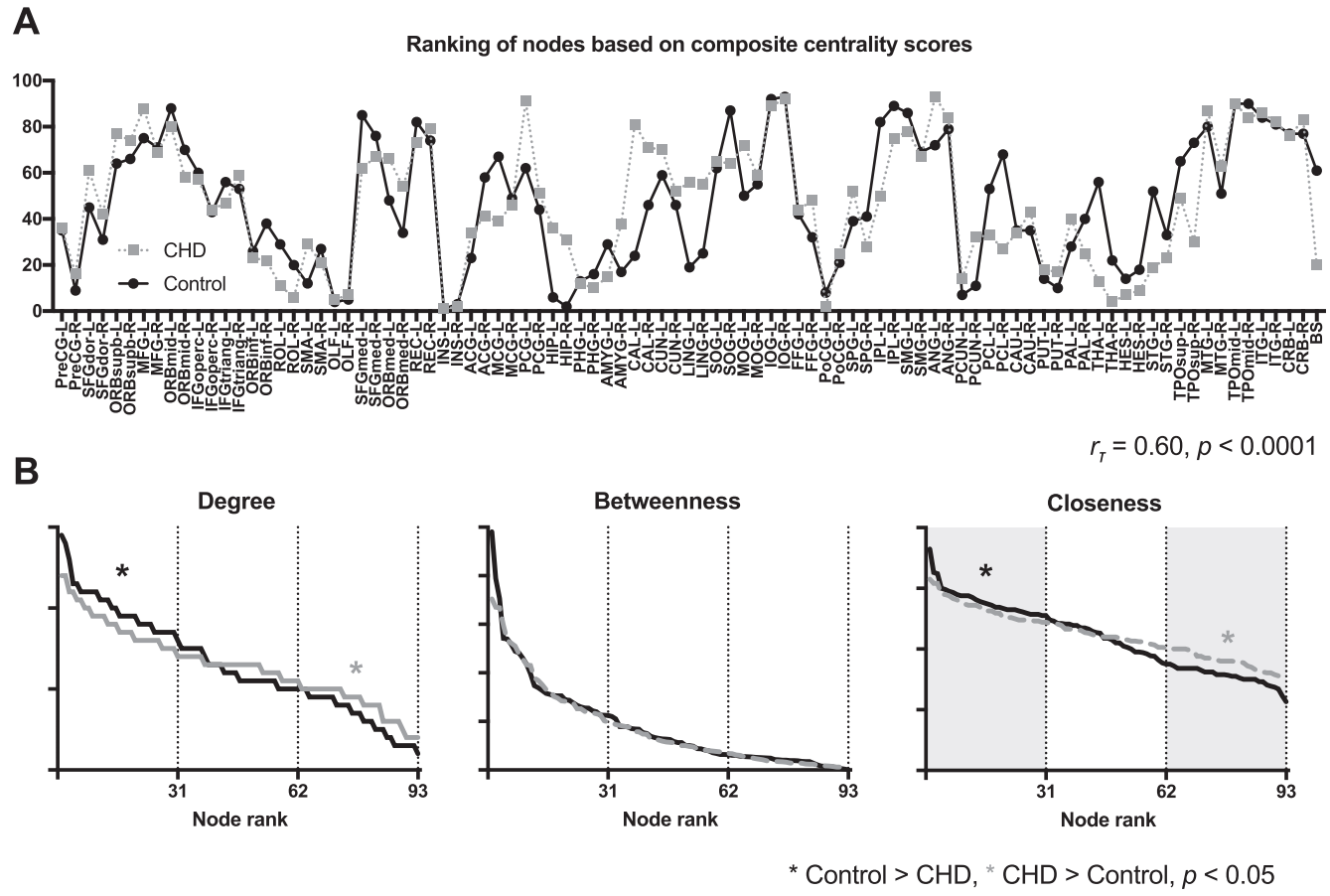

Fig. 4. Network hubs in CHD and controls. (A) Nodes ranked highly in controls (black, solid line) were also ranked highly in CHD (gray, dashed line). (B) While node rankings were similar, the degree and closeness of the most influential nodes (ranked in the top third) were higher in controls compared to CHD.

brainstem, over half (62%) of affected edges were interhemispheric. Most of the aberrant connections (78%) involved rich club nodes. Among the 60 affected edges, 15 (25%) were between two rich club nodes and 32 (53%) involved one rich club node. We did not observe any connections that were stronger in CHD compared to controls. We also compared CHD neonates with single- (1V) versus two-ventricle (2V) physiology and found no significant differences in regional functional connectivity between the two groups.

We then evaluated the functional connectedness of the affected regions against (1) the other nodes in the subnetwork, and (2) against the rest of the brain. Functional connectivity among the 30 involved nodes was significantly reduced in CHD compared to controls (Fig. 7). The average functional correlation in CHD was 0.14 ± 0.048 (Fisher z-transformed *r*) compared to 0.20 ± 0.084 in controls. Affected nodes' correlation with the rest of the brain, including regions outside the subnetwork, was also decreased in CHD compared with controls: CHD, 0.099 ± 0.04 versus controls, 0.14 ± 0.067 (p = 0.04).

4. Discussion

In this study, we demonstrated for the first time functional connectivity disturbances in resting state networks of neonates with complex CHD prior to surgery. Resting state networks in CHD, like controls, showed an efficient and economic small world architecture. While global network organization was preserved, regional (i.e. intermediate and local) network functional connectivity was perturbed in newborns with CHD. Rich club organization was intact in CHD networks but fewer nodes comprised the CHD rich club. Moreover, the density of connections among rich club nodes was reduced compared to healthy controls. Influential nodes in the CHD and control functional connectivity networks were similar, however, hubs in control networks tended to be more highly connected and closer to other nodes. These rich club nodes and/or hubs were predominantly involved in a subnetwork of regions with diminished functional connectivity in CHD.

We report that global network organization is preserved in CHD. Our analysis showed comparable small world indices, global efficiency and cost-efficiency between CHD and control newborns. These data suggest that, amidst the background of fetal, transitional and early postnatal hemodynamic disturbances related to CHD, the brain's ability to efficiently transfer information among neighboring areas and across distant regions at minimal cost is maintained. Although unexpected, these results are consistent with what recent studies have shown about the resilience of the newborn brain to targeted attacks on critical brain regions or hubs (De Asis-Cruz et al., 2015; Gao et al., 2011). Compared to random and regular brain networks, small world brain networks in newborns, like adults (Achard et al., 2006), tolerate insults (i.e. brain injury) well, requiring removal of ~40% of nodes (in a 90-node network) before marked network disintegration and reductions in global efficiency ensue.

Altered global network topology has previously been reported in adolescents with D-transposition of the great arteries (D-TGA) repaired in early infancy with the arterial switch operation. A recent DTI study revealed increased '*small-worldness*' and reduced global efficiency (trend level) compared to controls, changes that were associated with neurocognitive outcomes observed in the cohort (Panigrahy et al., 2015). While these findings may appear inconsistent, it is possible that these findings reflect a disease continuum of neurodevelopmental outcome in CHD. We speculate that our findings reflect the brain's early response to perturbations in cerebral blood flow and in the D-TGA study the results may represent the cumulative, long-term effects of altered

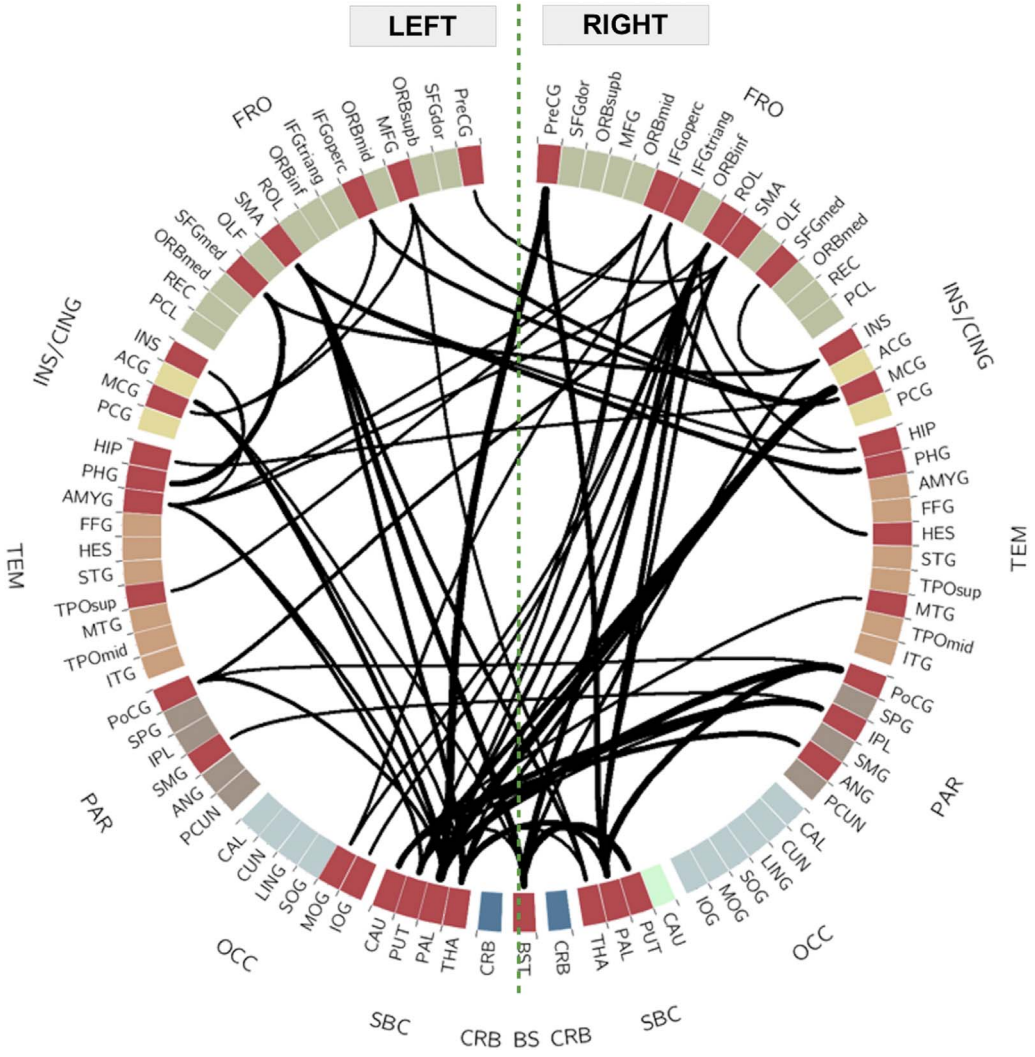

Fig. 5. Reduced connectivity in a subnetwork of nodes in CHD. Regions of interest divided by lobe: frontal (FRO), green; insula and cingulate (INS/CING), yellow; temporal (TEM) orange; parietal (PAR), brown; occipital (OCC), light blue; subcortical (SBC), light green; cerebellum (CRB), dark blue; and, brainstem (BS), black. Affected regions (red wedges) and edges (solid black lines) are shown. Thickness of connections reflect *t* statistic value. (For interpretation of the references to color in this figure legend, the reader is referred to the web version of this article.)

cerebral perfusion and the neurologic sequelae associated with cardiac surgery. While the onset, evolution, and relationship of global network changes in CHD neurobehavioral are yet to be elucidated, the intact efficient small world networks during early infancy suggests opportunities for targeted early therapeutic and rehabilitative interventions that could potentially minimize adverse long-term neurodevelopmental consequences.

While global network parameters were comparable between the two groups, regional analysis revealed functional disturbances in a subnetwork of nodes in newborns with CHD. In this subset of nodes, the majority of which were rich club or influential hubs, select connections showed reduced functional connectivity relative to controls. The subcortical regions including the bilateral putamen, caudate, globus pallidus, and thalamus were involved in most of these affected connections. Subcortical involvement in CHD has previously been reported. In fetuses with hypoplastic left heart syndrome (HLHS), Clouchoux et al. described reduced subcortical volume along with cortical gray and white matter volume decreases (Clouchoux et al., 2013). In the current study, our brain regions with reduced connectivity overlap with some of the areas previously shown to be delayed or reduced sulcation and gyrification in HLHS. The cingulate sulcus, frontal sulcus and anterior ascending ramus develop later in fetuses with HLHS. These sulci bound regions showed altered functional connectivity in neonates with CHD such as the middle cingulate, left mid- to superior frontal gyri, and right Rolandic operculum. Other affected sulci included the postcentral sulcus, collateral sulcus, superior temporal sulcus, and the Sylvian fissure. These sulci are closely related to the nodes in our dysconnected subnetwork – the postcentral sulcus borders the postcentral gyri and inferior parietal lobule, the collateral sulcus forms the lateral boundary of the parahippocampal gyrus, the superior temporal sulcus borders the middle temporal gyrus superiorly and meets the angular and supramarginal gyri posteriorly, and the Sylvian fissure and related sulci are closely related to the Rolandic operculum and inferior frontal gyrus. Apart from an ill-defined postcentral sulcus, reduced cortical depth in the postcentral region was also reported. Overall, the pattern of affected nodes mainly involved regions along the Sylvian fissure, postcentral gyrus, subcortical areas, and inferiorly, the parahippocampal regions.

In our study, regions that showed reduced functional connectivity corroborate previous findings of regional abnormalities described using MRS and DTI (Miller et al., 2007). Miller and colleagues reported reduced NAA/choline ratio in subcortical areas (i.e. basal ganglia and thalamus) in newborns with CHD before surgery compared to controls. In the same areas, they also reported increased average diffusivity and reduced FA. MRS and DTI revealed similar findings in the frontal and perirolandic white matter regions. Similar to the affected regions in our study, DTI findings of Rivkin et al. (2013) showed involvement of the midbrain, frontal cortices (i.e. right frontal/precentral gyri and insula), parietal areas, and temporal regions. Microstructural abnormalities in these areas spatially coincide with reduced functional connectivity in the midbrain, mid- and superior medial frontal gyrus, precentral gyrus, insula, intraparietal lobule, middle temporal gyrus and hippocampus. Decreases in FA in some of these regions including the right precentral

Table 2
Subnetwork with reduced connectivity in CHD.

Affected nodes			Aberrant edges							
	Node	*k*		Node 1	Node 2	*t*		Node 1	Node 2	*t*
1	PAL-L	11	1	INS-L	PHG-L	4.56	48	IPL-R	PAL-L	3.12
2	ROL-R	7	2	INS-L	AMYG-L	4.13	49	MCG-L	BS	3.12
3	BS	7	3	MCG-R	PAL-L	4.08	50	MFG-L	MCG-L	3.11
4	THA-L	6	4	PoCG-R	PAL-L	3.98	51	IFGoperc-R	AMYG-L	3.11
5	MCG-R	6	5	PreCG-R	PAL-L	3.84	52	IFGoperc-R	PUT-L	3.08
6	AMYG-L	5	6	PoCG-R	PAL-R	3.83	53	THA-L	THA-R	3.08
7	PUT-L	5	7	ROL-R	BS	3.83	54	IPL-R	SMG-L	3.06
8	PAL-R	5	8	SMA-L	BS	3.78	55	PAL-L	BS	3.06
9	SMA-L	5	9	IPL-R	CAU-L	3.76	56	IPL-R	PUT-L	3.05
10	MCG-L	5	10	SFGmed-L	PHG-L	3.72	57	IFGtriang-R	MOG-L	3.03
11	SMA-R	4	11	MCG-R	PUT-L	3.72	58	SMA-R	THA-L	3.03
12	IFGoperc-R	4	12	PUT-R	THA-L	3.69	59	MCG-R	HIP-L	3.01
13	IPL-R	4	13	PUT-R	BS	3.69	60	ROL-R	MOG-L	3
14	INS-R	3	14	PreCG-R	PAL-R	3.67	61	IPL-R	PAL-L	3.12
15	PoCG-L	3	15	PAL-R	BS	3.67	62	MCG-L	BS	3.12
16	THA-R	3	16	ROL-R	PAL-R	3.66	63	MFG-L	MCG-L	3.11
17	PoCG-R	3	17	SMA-L	PHG-R	3.63	64	IFGoperc-R	AMYG-L	3.11
18	CAU-L	3	18	MCG-L	PAL-L	3.59	65	IFGoperc-R	PUT-L	3.08
19	MFG-L	3	19	SMA-L	THA-L	3.55	66	THA-L	THA-R	3.08
20	INS-L	2	20	ANG-R	CAU-L	3.54	67	IPL-R	SMG-L	3.06
21	PHG-L	2	21	ROL-R	PAL-L	3.53	68	PAL-L	BS	3.06
22	PreCG-R	2	22	MCG-R	THA-L	3.53	69	IPL-R	PUT-L	3.05
23	PUT-R	2	23	IFGoperc-L	MCG-R	3.52	70	IFGtriang-R	MOG-L	3.03
24	HIP-R	2	24	MFG-L	MCG-R	3.43	71	SMA-R	THA-L	3.03
25	IFGoperc-L	2	25	SMA-L	THA-R	3.42	72	MCG-R	HIP-L	3.01
26	IFGtriang-R	2	26	SFGmed-L	INS-R	3.41	73	ROL-R	MOG-L	3
27	SFGmed-L	2	27	PoCG-L	PAL-L	3.4	74	IPL-R	PAL-L	3.12
28	MOG-L	2	28	INS-R	BS	3.39	75	MCG-L	BS	3.12
29	HES-R	1	29	AMYG-L	PUT-L	3.39	76	MFG-L	MCG-L	3.11
30	PHG-R	1	30	SMA-R	PoCG-L	3.35	77	IFGoperc-R	AMYG-L	3.11
31	IOG-L	1	31	SMA-R	PAL-R	3.33	78	IFGoperc-R	PUT-L	3.08
32	HIP-L	1	32	AMYG-L	PAL-L	3.31	79	THA-L	THA-R	3.08
33	PreCG-L	1	33	IFGtriang-R	HES-R	3.29	80	IPL-R	SMG-L	3.06
34	TPOsup-L	1	34	MCG-L	THA-L	3.29	81	PAL-L	BS	3.06
35	MTG-R	1	35	SFGmed-R	INS-R	3.27	82	IPL-R	PUT-L	3.05
36	SFGmed-R	1	36	SMA-L	HIP-R	3.27	83	IFGtriang-R	MOG-L	3.03
37	SMG-L	1	37	PreCG-L	SMA-R	3.23	84	SMA-R	THA-L	3.03
38	ANG-R	1	38	PoCG-L	PoCG-R	3.23	85	MCG-R	HIP-L	3.01
			39	IFGoperc-R	TPOsup-L	3.22	86	ROL-R	MOG-L	3
			40	IFGoperc-L	MCG-L	3.19	87	IPL-R	PAL-L	3.12
			41	ROL-R	HIP-R	3.19	88	MCG-L	BS	3.12
			42	CAU-L	MTG-R	3.19	89	MFG-L	MCG-L	3.11
			43	IFGoperc-R	PAL-L	3.18	90	IFGoperc-R	AMYG-L	3.11
			44	MFG-L	THA-R	3.16	91	IFGoperc-R	PUT-L	3.08
			45	ROL-R	IOG-L	3.15	92	THA-L	THA-R	3.08
			46	ROL-R	AMYG-L	3.15	93	IPL-R	SMG-L	3.06
			47	PUT-L	PAL-L	3.13				

k, degree; *t*, t statistic.

and right frontal regions correlated with impairments in higher-cognitive skills such as executive function and attention in adolescents with CHD (Rollins et al., 2014).

Taken together, the similarity between our findings in newborns and structural, MRS and DTI abnormalities identified during the fetal and early postnatal periods suggest that the connectivity disturbances reported in CHD infants are likely consequences of brain injury and/or delayed brain development that originated during the prenatal period. The temporal onset of functional changes, however, needs to be further elucidated. Whether these alterations in functional connectivity precede, coincide, or follow structural changes is an intriguing question that is actively being investigated in our laboratory and others.

The diffuse pattern of network alterations reported in our study is consistent with diffuse white matter abnormalities observed in newborns using DTI (Miller et al., 2007), and also, the global developmental disabilities observed in CHD. Although the neurological impairments reported in survivors of CHD are wide-ranging, executive dysfunction is prevalent and increasingly reported in this high-risk population. Deficits in higher-order cognitive function are especially relevant as they significantly impact long-term functional outcomes (Calderon and Bellinger, 2015). How atypical connectivity during early infancy in regions associated with executive functioning such as the subcortical and fronto-parietal regions in CHD relate to long-term functional disabilities remain to be fully explored. Nevertheless, related to DTI, the pattern of diffuse white matter microstructural injury (i.e., higher average diffusivity, and decreased white matter FA) in newborns with HLHS and d-TGA prior to cardiac surgery is reminiscent of the white matter changes in prematurity (Miller et al., 2007), suggesting delayed brain development in CHD. We posit that the reduced functional correlations among a group of regions in the brain may also reflect lack of maturity. Smyser et al. (2010), using seed based correlation analysis, reported weaker connectivity to the contralateral thalamus and sensorimotor cortex in 28 preterm infants with minimal brain injury scanned at 38–40 weeks PMA compared to term controls. This is consistent with the weaker functional connectivity between right and left thalamus and between the right thalamus and left SMA observed in our

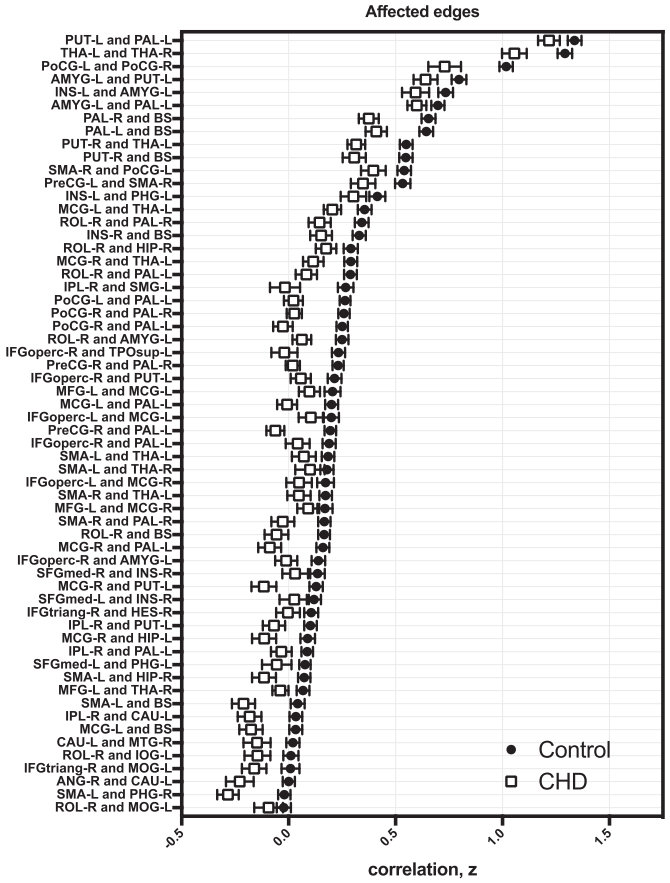

Fig. 6. Aberrant edges in CHD. Functional correlations between affected regions (transformed Fisher-z) were reduced in CHD (clear squares) compared to controls (filled circles); error bars show standard error of the mean.

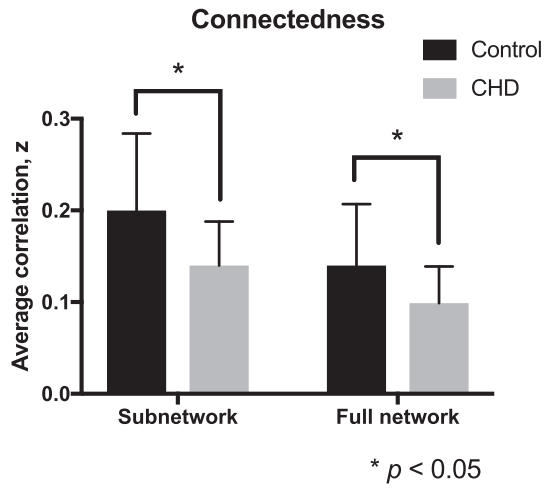

Fig. 7. Connectedness within subnetwork and full network. Neonates with CHD (gray) show reduced connectivity with other regions in the subnetwork (38 nodes) compared to healthy counterparts (gray). Correlations of affected regions with the rest of the brain (93 nodes) were also reduced in CHD.

cohort. In the same study, longitudinal analysis of 5 premature newborns at 30, 34 and 38 weeks GA also showed age-dependent increases in functional connectivity in their regions of interest, suggesting that increased functional correlations is a sign of brain maturity in early infancy. Related to this, increased density of connections among rich club nodes has been previously shown to be associated with increased gestational age in newborns (Ball et al., 2014). The decreased connectivity among rich club hubs that we described further suggests immaturity in the CHD brain.

NBS results also showed that the majority of affected edges (62%) connect to the contralateral hemisphere. The number of affected regions per hemisphere was almost equal: 19 on the left and 18 on the right. The more robust differences (thicker lines in Fig. 5) seemed to emerge from the left subcortical areas to the right cortex. This may be suggestive of significant lateralization differences that warrant further examination on a larger, more homogenous sample of CHD newborns.

The findings in our study should be interpreted in the context of the following limitations. First, while all patients had complex CHD requiring neonatal surgery, our CHD diagnostic groups were heterogeneous. Anatomical abnormalities, pathophysiology, and likely, molecular or genetic origins of these lesions vary. These differences may be reflected in the brain's network organization. A larger sample size is needed to delineate CHD diagnosis-specific network changes. Here, instead, we have focused on elucidating network alterations common to complex CHD, meaning the changes that arise from the shared hemodynamic instability during the fetal and early postnatal periods. We should note, however, that initial analyses using NBS showed no differences in regional connectivity between infants with single- and two-ventricle physiology, suggesting that impaired functional connectivity may not be specific to CHD diagnosis but rather more generalizable to the broader cohort of newborns with critical heart disease necessitating neonatal cardiac surgery. We postulate that a more nuanced picture of functional connectivity may emerge from studying larger cohorts with homogenous diagnoses. Second, while the majority of our MRI studies in newborns with CHD were unsedated, three were sedated for clinical reasons during their pre-operative scan. The effects of sedation and anesthesia on resting state networks are not fully understood. Based on recent studies in premature newborns (Damaraju et al., 2010; Doria et al., 2010), comparable resting state connectivity has been described in sedated and non-sedated groups. Given that very few newborns (n = 3) were sedated in our CHD cohort, we were unable to meaningfully compare whether there were differences in functional connectivity between those that were sedated and those that were not We posit that the influence of sedation on our results was minimal, at most. Nevertheless to precisely address the influence of sedation on connectivity in the developing brain, future studies that systematically investigate brain functional interactions under sedation in newborns are needed. Third, in the interest of providing an exhaustive yet concise comparison of network topology in healthy newborns and infants with CHD, only select global, intermediate, and nodal metrics were reported. Metrics that have been shown to be altered in CHD populations (i.e. modularity) and in neurodevelopmental diseases highly associated with CHD (i.e. participation coefficient) need to be further explored in newborns (Panigrahy et al., 2015; Shi et al., 2013). Similar to other fc-MRI studies, we examined the temporal correlation of BOLD signals between different areas of the brain rather than physical connections, i.e., white matter tracts. While studies in adults (Damoiseaux and Greicius, 2009) and infants (van den Heuvel et al., 2015) show overlap between functional and anatomical connectivity, an empirical account of their relationship during the first four weeks of life would provide further insights.

We report for the first time, alterations in resting state functional connectivity in neonates with complex CHD before surgery in the absence of brain parenchymal injury. Global network organization in the CHD neonate brain prior to surgery was preserved. CHD resting state networks demonstrated small-world properties of efficiency and economy. Regional disturbances, however, were observed in a subset of nodes, with marked involvement of subcortical regions and the brainstem. The spatial pattern of involvement is in keeping with the distribution of structural and metabolic findings using fetal morphometry, DTI and MRS and provides the first evidence of functional resting state network alterations after birth but before surgery in CHD infants. Our findings highlight the presence of early-life neural connectivity

disturbances in newborns with complex CHD prior to open heart surgery, and suggest that rs-fMRI may serve as a potential early biomarker of functional alterations and carries important implications for targeted early intervention services in this high-risk population.

Supplementary data to this article can be found online at https://doi.org/10.1016/j.nicl.2017.09.020.

Funding

This work is supported by the National Institutes of Health R01 HL116585-01 (CL) and the Canadian Institutes of Health Research MOP-81116 (CL).

Acknowledgements

We would like to thank Samantha Bauer and Diane Lanham for recruiting and coordinating family visits, Kushal Kapse for acquiring data and assisting with data quality assurance. We would like to thank the families who participated in this study.

References

Achard, S., Bullmore, E., 2007. Efficiency and cost of economical brain functional networks. PLoS Comput. Biol. 3, e17. http://dx.doi.org/10.1371/journal.pcbi.0030017.

Achard, S., Salvador, R., Whitcher, B., Suckling, J., Bullmore, E., 2006. A resilient, low-frequency, small-world human brain functional network with highly connected association cortical hubs. J. Neurosci. 26, 63–72. http://dx.doi.org/10.1523/JNEUROSCI.3874-05.2006.

Ball, G., Aljabar, P., Zebari, S., Tusor, N., Arichi, T., Merchant, N., Robinson, E.C., Ogundipe, E., Rueckert, D., Edwards, A.D., Counsell, S.J., 2014. Rich-club organization of the newborn human brain. Proc. Natl. Acad. Sci. 111, 7456–7461. http://dx.doi.org/10.1073/pnas.1324118111.

Bassett, D.S., Bullmore, E.T., 2009. Human brain networks in health and disease. Curr. Opin. Neurol. 22, 340–347. http://dx.doi.org/10.1097/WCO.0b013e32832d93dd.

Bassett, D.S., Meyer-Lindenberg, A., Achard, S., Duke, T., Bullmore, E., 2006. Adaptive reconfiguration of fractal small-world human brain functional networks. Proc. Natl. Acad. Sci. 103, 19518–19523. http://dx.doi.org/10.1073/pnas.0606005103.

Beall, E.B., Lowe, M.J., 2014. SimPACE: generating simulated motion corrupted BOLD data with synthetic-navigated acquisition for the development and evaluation of SLOMOCO: a new, highly effective slicewise motion correction. NeuroImage 101, 21–34. http://dx.doi.org/10.1016/j.neuroimage.2014.06.038.

Bellinger, D.C., Jonas, R.A., Rappaport, L.A., Wypij, D., Wernovsky, G., Kuban, K.C., Barnes, P.D., Holmes, G.L., Hickey, P.R., Strand, R.D., 1995. Developmental and neurologic status of children after heart surgery with hypothermic circulatory arrest or low-flow cardiopulmonary bypass. N. Engl. J. Med. 332, 549–555. http://dx.doi.org/10.1056/NEJM199503023320901.

Biswal, B., Yetkin, F.Z., Haughton, V.M., Hyde, J.S., 1995. Functional connectivity in the motor cortex of resting human brain using echo-planar MRI. Magn. Reson. Med. 34, 537–541.

Calderon, J., Bellinger, D.C., 2015. Executive function deficits in congenital heart disease: why is intervention important? CTY 25, 1238–1246. http://dx.doi.org/10.1017/S1047951115001134.

Clouchoux, C., du Plessis, A.J., Bouyssi-Kobar, M., Tworetzky, W., McElhinney, D.B., Brown, D.W., Gholipour, A., Kudelski, D., Warfield, S.K., McCarter, R.J., Robertson, R.L., Evans, A.C., Newburger, J.W., Limperopoulos, C., 2013. Delayed cortical development in fetuses with complex congenital heart disease. Cereb. Cortex 23, 2932–2943. http://dx.doi.org/10.1093/cercor/bhs281.

Colizza, V., Flammini, A., Serrano, M.A., Vespignani, A., 2006. Detecting rich-club ordering in complex networks. Nat. Phys. 2, 110–115. http://dx.doi.org/10.1038/nphys209.

Cox, R.W., 1996. AFNI: software for analysis and visualization of functional magnetic resonance neuroimages. Comput. Biomed. Res. 29, 162–173.

Damaraju, E., Phillips, J.R., Lowe, J.R., Ohls, R., Calhoun, V.D., Caprihan, A., 2010. Resting-state functional connectivity differences in premature children. Front. Syst. Neurosci. 4.

Damoiseaux, J.S., Greicius, M.D., 2009. Greater than the sum of its parts: a review of studies combining structural connectivity and resting-state functional connectivity. Brain Struct. Funct. 213, 525–533. http://dx.doi.org/10.1007/s00429-009-0208-6.

De Asis-Cruz, J., Bouyssi-Kobar, M., Evangelou, I., Vezina, G., Limperopoulos, C., 2015. Functional properties of resting state networks in healthy full-term newborns. Sci Rep 5, 17755. http://dx.doi.org/10.1038/srep17755.

Donofrio, M.T., Massaro, A.N., 2010. Impact of congenital heart disease on brain development and neurodevelopmental outcome. Int. J. Pediatr. 2010, 1–13. http://dx.doi.org/10.1155/2010/359390.

Doria, V., Beckmann, C.F., Arichi, T., Merchant, N., Groppo, M., Turkheimer, F.E., Counsell, S.J., Murgasova, M., Aljabar, P., Nunes, R.G., Larkman, D.J., Rees, G., Edwards, A.D., 2010. Emergence of resting state networks in the preterm human brain. Proc. Natl. Acad. Sci. U. S. A. 107, 20015–20020.

Fransson, P., Aden, U., Blennow, M., Lagercrantz, H., 2011. The functional architecture of the infant brain as revealed by resting-state fMRI. Cereb. Cortex 21, 145–154. http://dx.doi.org/10.1093/cercor/bhq071.

Freeman, L.C., 1978. Centrality in social networks conceptual clarification. Soc. Networks 1, 215–239.

Freeman, L.C., Borgatti, S.P., White, D.R., 1991. Centrality in valued graphs: a measure of betweenness based on network flow. Soc. Networks 13, 141–154. http://dx.doi.org/10.1016/0378-8733(91)90017-N.

Gao, W., Gilmore, J.H., Giovanello, K.S., Smith, J.K., Shen, D., Zhu, H., Lin, W., 2011. Temporal and spatial evolution of brain network topology during the first two years of life. PLoS ONE 6, e25278–13. http://dx.doi.org/10.1371/journal.pone.0025278.

Gaynor, J.W., Stopp, C., Wypij, D., Andropoulos, D.B., Atallah, J., Atz, A.M., Beca, J., Donofrio, M.T., Duncan, K., Ghanayem, N.S., Goldberg, C.S., Hövels-Gürich, H., Ichida, F., Jacobs, J.P., Justo, R., Latal, B., Li, J.S., Mahle, W.T., McQuillen, P.S., Menon, S.C., Pemberton, V.L., Pike, N.A., Pizarro, C., Shekerdemian, L.S., Synnes, A., Williams, I., Bellinger, D.C., Newburger, J.W., International Cardiac Collaborative on Neurodevelopment (ICCON) Investigators, 2015. Neurodevelopmental outcomes after cardiac surgery in infancy. Pediatrics 135, 816–825. http://dx.doi.org/10.1542/peds.2014-3825.

Gong, G., HE, Y., Evans, A.C., 2011. Brain connectivity: gender makes a difference. Neuroscientist 17, 575–591. http://dx.doi.org/10.1177/1073858410386492.

Hallquist, M.N., Hwang, K., Luna, B., 2013. The nuisance of nuisance regression: spectral misspecification in a common approach to resting-state fMRI preprocessing reintroduces noise and obscures functional connectivity. NeuroImage 82, 208–225. http://dx.doi.org/10.1016/j.neuroimage.2013.05.116.

van den Heuvel, M.P., Sporns, O., 2011. Rich-club organization of the human connectome. J. Neurosci. 31, 15775–15786. http://dx.doi.org/10.1523/JNEUROSCI.3539-11.2011.

van den Heuvel, M.P., Sporns, O., 2013. Network hubs in the human brain. Trends Cogn. Sci. 17, 683–696. http://dx.doi.org/10.1016/j.tics.2013.09.012.

van den Heuvel, M.P., Kersbergen, K.J., de Reus, M.A., Keunen, K., Kahn, R.S., Groenendaal, F., de Vries, L.S., Benders, M.J.N.L., 2015. The neonatal connectome during preterm brain development. Cereb. Cortex 25, 3000–3013. http://dx.doi.org/10.1093/cercor/bhu095.

Hövels-Gürich, H.H., Konrad, K., Wiesner, M., Minkenberg, R., Herpertz-Dahlmann, B., Messmer, B.J., Von Bernuth, G., 2002. Long term behavioural outcome after neonatal arterial switch operation for transposition of the great arteries. Arch. Dis. Child. 87, 506–510. http://dx.doi.org/10.1136/adc.87.6.506.

Humphries, M.D., Gurney, K., 2008. Network "small-world-ness": a quantitative method for determining canonical network equivalence. PLoS ONE 3, e0002051. http://dx.doi.org/10.1371/journal.pone.0002051.

Humphries, M.D., Gurney, K., Prescott, T.J., 2006. The brainstem reticular formation is a small-world, not scale-free, network. Proc. R. Soc. B Biol. Sci. 273, 503–511. http://dx.doi.org/10.1098/rspb.2005.3354.

Itahashi, T., Yamada, T., Watanabe, H., Nakamura, M., Jimbo, D., Shioda, S., Toriizuka, K., Kato, N., Hashimoto, R., 2014. Altered network topologies and hub organization in adults with autism: a resting-state fMRI study. PLoS ONE 9, e94115–15. http://dx.doi.org/10.1371/journal.pone.0094115.

Jo, H.J., Gotts, S.J., Reynolds, R.C., Bandettini, P.A., Martin, A., Cox, R.W., Saad, Z.S., 2013. Effective preprocessing procedures virtually eliminate distance-dependent motion artifacts in resting state FMRI. J. Appl. Math. 2013, 1–9. http://dx.doi.org/10.1155/2013/935154.

Limperopoulos, C., Majnemer, A., Shevell, M.I., Rosenblatt, B., Rohlicek, C., Tchervenkov, C., 1999. Neurologic status of newborns with congenital heart defects before open heart surgery. Pediatrics 103, 402–408.

Limperopoulos, C., Majnemer, A., Shevell, M.I., Rohlicek, C., Rosenblatt, B., Tchervenkov, C., Darwish, H.Z., 2002. Predictors of developmental disabilities after open heart surgery in young children with congenital heart defects. J. Pediatr. 141, 51–58. http://dx.doi.org/10.1067/mpd.2002.125227.

Limperopoulos, C., Tworetzky, W., McElhinney, D.B., Newburger, J.W., Brown, D.W., Robertson, R.L., Guizard, N., McGrath, E., Geva, J., Annese, D., Dunbar-Masterson, C., Trainor, B., Laussen, P.C., du Plessis, A.j., 2010. Brain volume and metabolism in fetuses with congenital heart disease: evaluation with quantitative magnetic resonance imaging and spectroscopy. Circulation 121, 26–33. http://dx.doi.org/10.1161/CIRCULATIONAHA.109.865568.

Lynall, M.-E., Bassett, D.S., Kerwin, R., McKenna, P.J., Kitzbichler, M., Muller, U., Bullmore, E., 2010. Functional connectivity and brain networks in schizophrenia. J. Neurosci. 30, 9477–9487. http://dx.doi.org/10.1523/JNEUROSCI.0333-10.2010.

Makropoulos, A., Gousias, I.S., Ledig, C., Aljabar, P., Serag, A., Hajnal, J.V., Edwards, A.D., Counsell, S.J., Rueckert, D., 2014. Automatic whole brain MRI segmentation of the developing neonatal brain. IEEE Trans. Med. Imaging 33, 1818–1831. http://dx.doi.org/10.1109/TMI.2014.2322280.

Marelli, A., Miller, S.P., Marino, B.S., Jefferson, A.L., Newburger, J.W., 2016. Brain in congenital heart disease across the lifespan: the cumulative burden of injury. Circulation 133, 1951–1962. http://dx.doi.org/10.1161/CIRCULATIONAHA.115.019881.

McQuillen, P.S., Barkovich, A.J., Hamrick, S.E.G., Perez, M., Ward, P., Glidden, D.V., Azakie, A., Karl, T., Miller, S.P., 2007. Temporal and anatomic risk profile of brain injury with neonatal repair of congenital heart defects. Stroke 38, 736–741. http://dx.doi.org/10.1161/01.STR.0000247941.41234.90.

Miller, S.P., McQuillen, P.S., Vigneron, D.B., Glidden, D.V., Barkovich, A.J., Ferriero, D.M., Hamrick, S.E.G., Azakie, A., Karl, T.R., 2004. Preoperative brain injury in newborns with transposition of the great arteries. Ann. Thorac. Surg. 77, 1698–1706. http://dx.doi.org/10.1016/j.athoracsur.2003.10.084.

Miller, S.P., McQuillen, P.S., Hamrick, S., Xu, D., Glidden, D.V., Charlton, N., Karl, T., Azakie, A., Ferriero, D.M., Barkovich, A.J., Vigneron, D.B., 2007. Abnormal brain development in newborns with congenital heart disease. N. Engl. J. Med. 357,

1928–1938. http://dx.doi.org/10.1056/NEJMoa067393.
Moseley, R.L., Ypma, R.J.F., Holt, R.J., Floris, D., Chura, L.R., Spencer, M.D., Baron-Cohen, S., Suckling, J., Bullmore, E., Rubinov, M., 2015. Whole-brain functional hypoconnectivity as an endophenotype of autism in adolescents. YNICL 9, 140–152. http://dx.doi.org/10.1016/j.nicl.2015.07.015.
Newman, M.F., Kirchner, J.L., Phillips-Bute, B., Gaver, V., Grocott, H., Jones, R.H., Mark, D.B., Reves, J.G., Blumenthal, J.A., Neurological Outcome Research Group and the Cardiothoracic Anesthesiology Research Endeavors Investigators, 2001. Longitudinal assessment of neurocognitive function after coronary-artery bypass surgery. N. Engl. J. Med. 344, 395–402. http://dx.doi.org/10.1056/NEJM200102083440601.
Ojemann, J.G., Akbudak, E., Snyder, A.Z., McKinstry, R.C., Raichle, M.E., Conturo, T.E., 1997. Anatomic localization and quantitative analysis of gradient refocused echo-planar fMRI susceptibility artifacts. NeuroImage 6, 156–167. http://dx.doi.org/10.1006/nimg.1997.0289.
Panigrahy, A., Schmithorst, V.J., Wisnowski, J.L., Watson, C.G., Bellinger, D.C., Newburger, J.W., Rivkin, M.J., 2015. Relationship of white matter network topology and cognitive outcome in adolescents with d-transposition of the great arteries. YNICL 7, 438–448. http://dx.doi.org/10.1016/j.nicl.2015.01.013.
Peer, M., Abboud, S., Hertz, U., Amedi, A., Arzy, S., 2016. Intensity-based masking: a tool to improve functional connectivity results of resting-state fMRI. Hum. Brain Mapp. 37, 2407–2418. http://dx.doi.org/10.1002/hbm.23182.
Power, J.D., Barnes, K.A., Snyder, A.Z., Schlaggar, B.L., Petersen, S.E., 2012. Spurious but systematic correlations in functional connectivity MRI networks arise from subject motion. NeuroImage 59, 2142–2154. http://dx.doi.org/10.1016/j.neuroimage.2011.10.018.
Rivkin, M.J., Watson, C.G., Scoppettuolo, L.A., Wypij, D., Vajapeyam, S., Bellinger, D.C., DeMaso, D.R., Robertson, R.L., Newburger, J.W., 2013. Adolescents with D-transposition of the great arteries repaired in early infancy demonstrate reduced white matter microstructure associated with clinical risk factors. J. Thorac. Cardiovasc. Surg. 146http://dx.doi.org/10.1016/j.jtcvs.2012.12.006. (543–9.e1).
Rollins, C.K., Watson, C.G., Asaro, L.A., Wypij, D., Vajapeyam, S., Bellinger, D.C., DeMaso, D.R., Robertson, R.L., Newburger, J.W., Rivkin, M.J., 2014. White matter microstructure and cognition in adolescents with congenital heart disease. J. Pediatr. 165http://dx.doi.org/10.1016/j.jpeds.2014.07.028. (936–44.e1–2).
Rubinov, M., Sporns, O., 2010. Complex network measures of brain connectivity: uses and interpretations. NeuroImage 52, 1059–1069. http://dx.doi.org/10.1016/j.neuroimage.2009.10.003.
Satterthwaite, T.D., Wolf, D.H., Loughead, J., Ruparel, K., Elliott, M.A., Hakonarson, H., Gur, R.C., Gur, R.E., 2012. Impact of in-scanner head motion on multiple measures of functional connectivity: relevance for studies of neurodevelopment in youth. NeuroImage 60, 623–632. http://dx.doi.org/10.1016/j.neuroimage.2011.12.063.
Shi, F., Yap, P.-T., Wu, G., Jia, H., Gilmore, J.H., Lin, W., Shen, D., 2011. Infant brain atlases from neonates to 1- and 2-year-olds. PLoS ONE 6, e18746. http://dx.doi.org/10.1371/journal.pone.0018746.
Shi, F., Wang, L., Peng, Z., Wee, C.Y., Shen, D., 2013. Altered modular organization of structural cortical networks in children with autism. PLoS ONE 8, e63131.
Smyser, C.D., Inder, T.E., Shimony, J.S., Hill, J.E., Degnan, A.J., Snyder, A.Z., Neil, J.J., 2010. Longitudinal analysis of neural network development in preterm infants. Cereb. Cortex 20, 2852–2862. http://dx.doi.org/10.1093/cercor/bhq035.
Tustison, N.J., Avants, B.B., Cook, P.A., Zheng, Yuanjie, Egan, A., Yushkevich, P.A., Gee, J.C., 2010. N4ITK: improved N3 bias correction. IEEE Trans. Med. Imaging 29, 1310–1320. http://dx.doi.org/10.1109/TMI.2010.2046908.
Watts, D.J., Strogatz, S.H., 1998. Collective dynamics of “small-world” networks. Nature 393, 440–442. http://dx.doi.org/10.1038/30918.
Xia, M., Wang, J., HE, Y., 2013. BrainNet Viewer: a network visualization tool for human brain connectomics. PLoS ONE 8, e68910. http://dx.doi.org/10.1371/journal.pone.0068910.
Zalesky, A., Fornito, A., Bullmore, E.T., 2010. Network-based statistic: identifying differences in brain networks. NeuroImage 53, 1197–1207. http://dx.doi.org/10.1016/j.neuroimage.2010.06.041.